Journal of Inorganic and Organometallic Polymers and Materials (2021) 31:4504–4511
https://doi.org/10.1007/s10904-021-02062-6

Carbon Nanoparticles on Magnetite: A New Heterogeneous Catalyst for the Oxidation of 5-Hydroxymethylfurfural (5-HMF) to 2,5-Diformoylfuran (DFF)

Rama Jaiswal[1] · **Kalluri V. S. Ranganath**[1]

Received: 3 May 2021 / Accepted: 24 June 2021 / Published online: 29 June 2021

Abstract
Development of new materials for catalytic applications is one of the rapidly growing research areas. The selective oxidation of 5-hydroxymethyl furfural (HMF) to 2,5-diformylfuran (DFF) is one of the rapidly growing research area due to having its own importance in the fuel technology. We report a new heterogeneous catalyst for the oxidation of HMF to DFF in aqueous medium using a carbon soot (from candle light) deposited on magnetite (Fe_3O_4@C). Further, the potentiality of our catalyst has also been realized in direct production of DFF from biomass (using either fructose or glucose) with high conversions via two consecutive steps involving dehydration and oxidation. Further, proved that Fe_3O_4@C plays a major role in the dehydration of sugar molecules whereas Fe_3O_4 alone could not.

Keywords Magnetite · Oxidation of HMF · Heterogeneous catalysis

1 Introduction

Due to rapid diminishing of fossil feedstock there is huge and enormous demand for sustainable and alternative sources of energy. Massive generation of biofuels from bio waste is one of the major challenging research areas to increase feedstock [1]. Transformation of biomass-derived 5-hydroxymethylfurfural (HMF) to value-added platform chemicals such as 2,5-Diformoyl furan (DFF) has been drastically increased during the past few decades due to having its own importance in fuel technology, polymers, in the synthesis of pharmaceuticals, fungicides and heterocyclic ligands [2–7]. The selective oxidation of 5-HMF to 2,5-DFF is quite difficult due to having the two reactive functional groups which can undergo different types of reactions such as hydrogenation, oxidations and hydrogenolysis of C-O bonds respectively [8]. Because of highly reactive functional groups, other furan derivatives such as 5-hydroxymethyl-2-furan carboxylic acid (HMFCA), 5-formyl-2-furancarboxylicacid (FFCA) and 2,5-furan-dicarboxylicacid (FDCA) were also formed during the oxidation reaction [9]. Therefore selective oxidation of 5-HMF to DFF under mild conditions is remaining challenged. In this direction, several researchers have reported the synthesis of DFF selectively from 5-HMF using a both homogeneous catalysts and very recently using copper salts [10]. There are several reports on the oxidation of 5-HMF to DFF using heterogeneous catalysts including Ru immobilized catalysts [11, 12], MnO_2 or metal doped MnO_2 catalysts [13–18]. In addition, vanadium on different supports such as graphitic nitride, carbon have been extensively used in the oxidation of 5-HMF to DFF in good yields [19–23]. Further, iron based heterogeneous catalysts are widely used in the oxidation reaction due to non-precious and easily available [24–27]. All these catalysts are used either in the presence of various oxidants with high concentrations (or) in highly polar solvents such as DMF and DMSO or at higher temperatures. Therefore the development of sustainable heterogeneous catalyst, efficient and cost effective catalytic protocol is highly desirable under the mild conditions.

Carbon based materials have been widely used in electronics, optics, drug delivery vehicles and in catalytic applications [28]. Since these materials exhibit unprecedented physical and chemical properties due to the inherent structural rearrangement, it has been used to fabricate the various composite materials like carbon/ceramic,

✉ Kalluri V. S. Ranganath
ranganath.chem@bhu.ac.in

[1] Department of Chemistry, Institute of Science, Banaras Hindu University, Varanasi, India

carbon/cement and carbon/metal composites and metal carbides [28–30]. However, synthesis of such carbon based materials is quite expensive and not easy to prepare using simple protocols in the laboratory. Carbon encapsulated magnetite materials have been previously reported using glucose as a carbon source [31–35]. In addition, uniform and hydrophobic carbon nanoparticles (CNPs) can be obtained from candle soot and considered as an essential components for various applications including sensors, quantum dots, electrocatalysts, energy storages, lubrication and functional coatings [36]. Synthesis of CNPs using candle soot is a simple technique, inexpensive and also another advantage is it take short period of time to prepare [37–39].

Herein we report the development of carbon nanoparticles (CNPs) embedded on magnetite (Fe_3O_4) for heterogeneous catalytic applications. It was prepared by a simple protocol using candle soot as a source of CNPs in the presence of ferric chloride and polyvinyl alcohol (PVA). The proposed synthesis is environmental friendly because of converting pollutant material, *i.e.* carbon particles to an active catalyst. The resultant solid (denoted as Fe_3O_4@C) was completely characterized using different techniques such as PXRD, XPS, Raman and SEM–EDX analysis (Fig. 1). *To the best of our knowledge CNPs or CNPs decorated materials have not been used in heterogeneous catalysis*.

The obtained Fe_3O_4@C has served as an active potential candidate in the oxidation of 5-HMF in aqueous medium [40]. We chose iron oxide for the preparation of Fe_3O_4@C due to its relatively non-toxic, abundant and possessing magnetic properties [41]. Therefore MNPs were selected to adsorb hydrophobic CNPs for the selective aerobic oxidation of 5-HMF as shown in the Scheme 1.

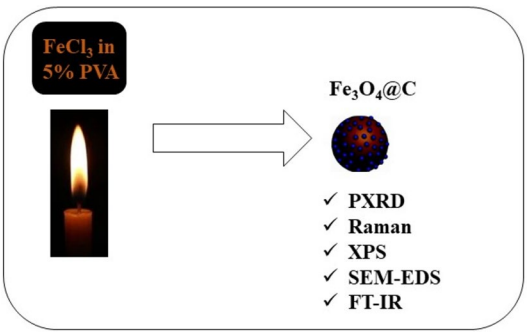

Fig. 1 Schematic diagram of preparation of carbon nanoparticles (CNPs) on Fe_3O_4

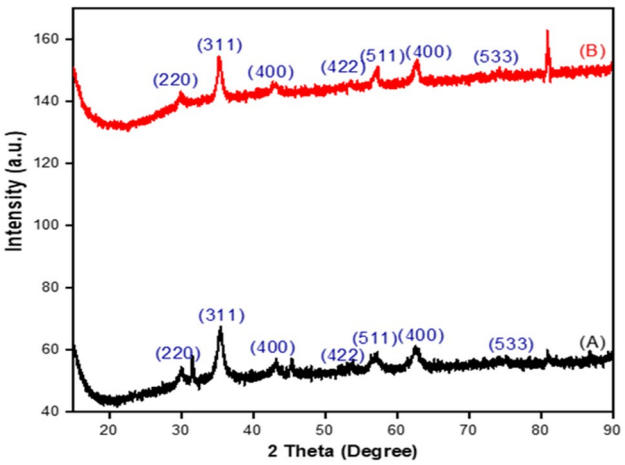

Fig. 2 PXRD Pattern of (A) Fe_3O_4 (B) Fe_3O_4@CNP

2 Experimental

2.1 Synthesis of Fe_3O_4@C

The aluminium plates and all chemicals were purchased from Sigma Aldrich. The aluminium plate was cut into square shaped disks (thickness = 1 mm, length = 20 mm). These disks were successively pre-treated by sonication using acetone, ethanol and Milli-Q water respectively. The $FeCl_3$ in 5% polyvinyl alcohol (PVA) were allowed to stick on the aluminium plate. Later, candle (diameter = 10 mm) was lighted and metal salt coated plate was placed near the tip of candle soot. The soot was deposited from the tip of the flame on the disks in the presence of iron chloride, polyvinyl alcohol and kept it for 30 min. In this protocol, carbon particles were deposited on iron oxide by (in situ) converting iron chloride to iron oxide. Later the brown solid was collected from plate and washed with acetone and Milli-Q water and dried in oven at 120 °C for 5 h. Raman spectroscopy and XPS analysis confirms the presence of CNPs on magnetite.

2.2 Catalytic Application of Fe_3O_4@C

The catalytic activity of the as-prepared Fe_3O_4@C catalyst was evaluated by the oxidation of HMF. To an oven dried flask containing catalyst (5.0 mg), HMF (0.25 mmol), base (potassium carbonate) (2.0 equiv.) and the solvent (5.0 mL) were added at room temperature. The reaction mixture was stirred at the required temperature. After completion of the reaction, (monitored by HPLC) catalyst was separated through centrifugation and washed with alcohol (ethanol) for further use. The conversion and selectivity's were calculated using HPLC.

Scheme 1 Oxidation of 5-HMF to DFF using Fe_3O_4@C in aqueous medium

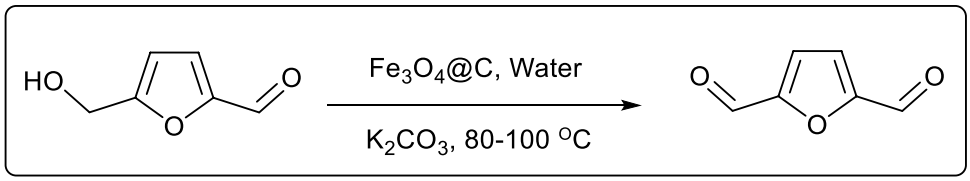

3 Characterization

The catalyst was characterized using different techniques like FT-IR, PXRD, SEM-FT-IR analysis of heterogeneous catalyst was carried out using PerkinElmer Spectrum. The crystallinity and phase analysis was performed using powder X-ray diffraction (PXRD) pattern. The PXRD pattern was recorded in a analytical High Resolution diffractometer equipped with Cu-Kα1 irradiation at a power of 40 kV × 40 mA (λ = 0.1542 nm). The chemical compositions were examined by Scanning Electron Microscopy equipped with energy dispersive x-ray (SEM–EDX) analysis using Carl Zeiss. X-ray photoelectron spectroscopic analysis (XPS) was performed using an ESCALAB250 instrument by Thermo VG Scientific. Unless stated otherwise, monochromatic Al Kα-radiation was used (15 kV, 150 W, ~ 500 µm spot diameter) with the transmission function of the analyzer having been calibrated using a standard copper sample. Reactions were monitored by HPLC from Shimadzu Company with dual pump using C-18 column using mobile phase: hexane: isopropanol (9:1).

4 Results and Discussion

4.1 Powdered X-ray Diffraction (PXRD)

The diffraction peaks of Fe_3O_4@C Bragg's angle appeared at 2θ ~ 30.3, 35.3, 43.1, 53.1, 57.1, 62.7, 74.2 corresponding to (220), (311), (400), (422), (511), (440) and (533) planes respectively. The data observed is attributed to Fe_3O_4 face centered cubic structure [JCPDS card No. 89-0950]. In the XRD pattern of Fe_3O_4@C, no additional peaks were observed except the peak broadening, which is attributed to due to the presence of CNPs on iron oxide (Fig. 2). The crystallite size was calculated by using Debye–Scherrer equation and found that 10.7 and 11.8 nm for pure magnetite and Fe_3O_4@C respectively (Fig. 2).

4.2 Fourier Transform Infrared (FT-IR) Analysis

FTIR spectrum of the Fe_3O_4@C shows a characteristic peak at nearly at 590 cm^{-1} denoting the presence of Fe–O bond (Fig. 3). Furthermore, several stretching frequencies associated with CNPs were observed at 1543 and 1634 cm^{-1} respectively. In addition, the broad stretching

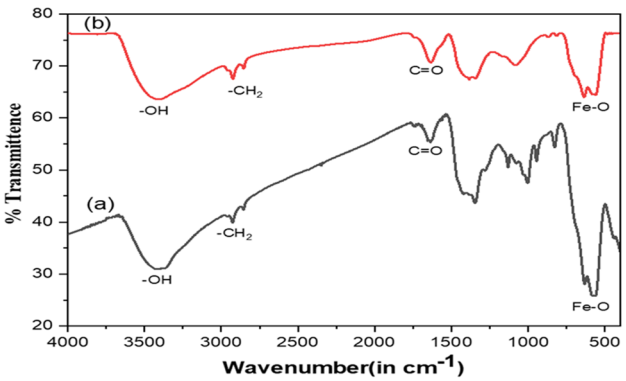

Fig. 3 FT-IR spectra of (a) Fe_3O_4 (b) Fe_3O_4@CNP

frequency at 3400–3850 cm^{-1} is attributed for the vibration of –OH group. These clearly illustrate that hydrophobic carbon particles are not adsorbed on surface of magnetite, they may be embedded inside the structure. The peaks at 3361 cm^{-1} and 1640 cm^{-1} corresponds to water of hydration of metal oxide NPs (Fig. 3).

4.3 X-ray Photo Electron Spectroscopy (XPS)

The heterogeneous active catalyst Fe_3O_4@C has further characterized by XPS (Fig. 1, Supporting Information, SI). The doublet profile of Fe_{2p} spectra into distinct $Fe2p_{3/2}$ and $Fe2p_{1/2}$ orbit at binding energies at 710.7 eV and 724.1 eV respectively. The stoichiometric magnetite Fe_3O_4 of cubic close packed oxygen sub lattice can be alternatively expressed as $FeO{\cdot}Fe_2O_3$. Therefore, it consists of both iron ions Fe^{2+} and Fe^{3+} occupying the tetrahedral and octahedral interstices of cubic spinel type structure. The O 1s binding energy at 532.22 eV corresponds to O^{2-} of Fe_3O_4 showing only one kind of oxygen species. It was identified to be the bridge oxygen (O) between octahedral iron (Fe^{3+}) and the tetrahedral (Fe^{2+}) lattice. Further binding energy for C 1s was observed at 284.12 eV, 293.15 eV and 295.62 eV respectively, which is indicating the presence of different carbon species. The peaks at low binding energies nearly at 284 eV, are ascribed to the lattice carbon atoms and the binding energies corresponding to CNPs

are 293 eV and at 296 eV oxidized carbons respectively (Fig. 1, SI).

4.4 Raman Spectroscopy

In addition, Fe_3O_4@C has also been characterized by Raman spectroscopy. In the present case, the Raman spectrum peaks of iron oxide (Fe_3O_4) were investigated and found that translator movement (T^1_{2g}) corresponding to FeO_4 are changed from 193 cm^{-1} of Fe_3O_4 to 214 cm^{-1} for CNP/Fe_3O_4 (Fig. 4). However, the asymmetric stretching (T^2_{2g}) and bending of Fe–O (T^3_{2g}) are remains same before and after incorporation of CNPs. Significantly, the symmetric bending of Fe–O of magnetite corresponding to E_g has been shifted from 319 to 279 cm^{-1} after incorporation of CNPs [42]. In addition, the peak at 680 cm^{-1} was identified as a band characteristic which was present on magnetite, however it has been disappeared in Fe_3O_4@C. This result further illustrate that hydrophobic CNPs have accommodated inside the magnetite, which may leads to the formation of crystal defects (Table 1).

4.5 SEM–EDS Analysis

The morphology and structural features of the Fe_3O_4@C has also been studied using scanning electron microscopy (SEM). Well defined spherical particles were observed approximately 20 nm and observed that all expected elements (Fe, O and C) are present on Fe_3O_4@C (Fig. 5).

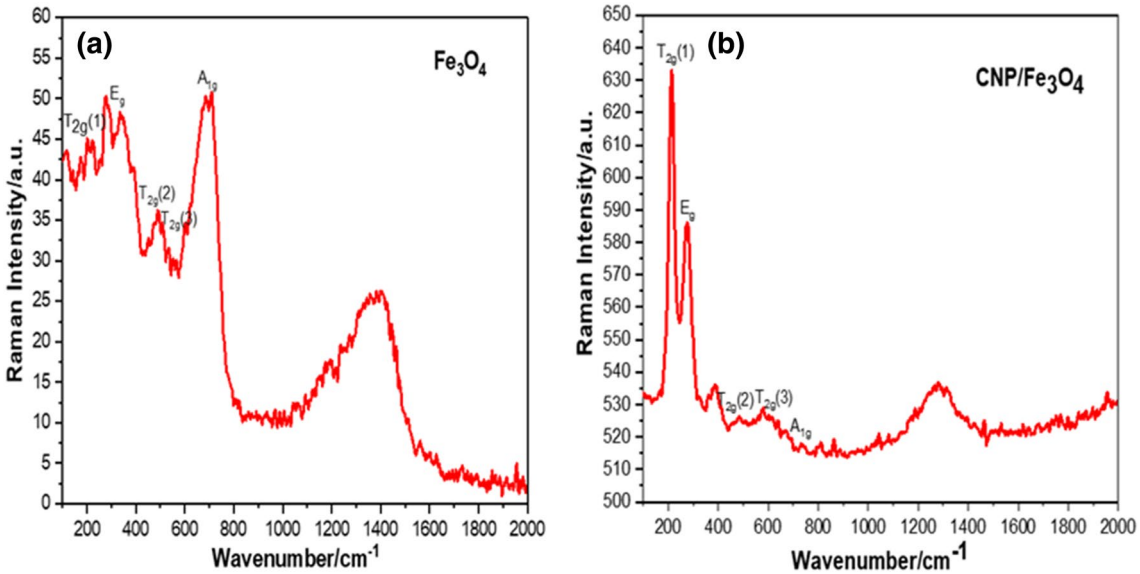

Fig. 4 Raman spectra of **a** Fe_3O_4, **b** Fe_3O_4/CNP

Table 1 Raman Shift Vibrations of Fe_3O_4 and Fe_3O_4@C

S. no	Vibrational mode	Fe_3O_4 (cm^{-1})	Fe_3O_4@C (cm^{-1})
1	T^1_{2g} (translatory movement of FeO_4)	193	214
2	T^2_{2g} (asymmetric stretch of Fe–O)	488	485
3	T^3_{2g} (asymmetric bend of Fe–O)	538	538
4	E_g (symmetric bend of Fe–O)	319	279
5	A_{1g} (symmetrical stretch of oxygen atoms along Fe–O)	683	670
6	Characteristic peak	1383	1286

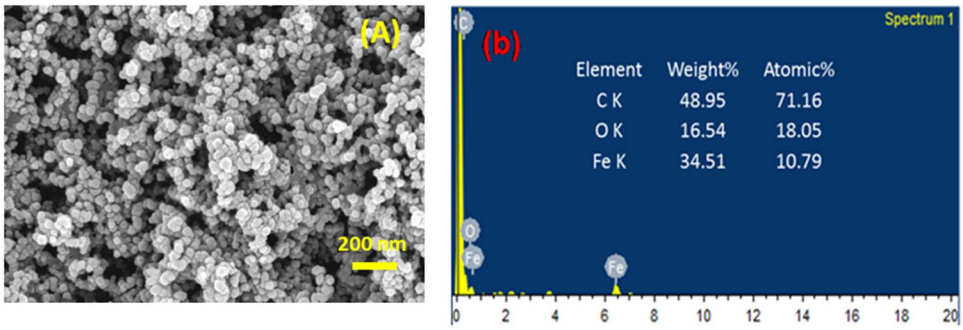

Fig. 5 SEM-EDS of Fe_3O_4/CNP

5 Heterogeneous Catalytic Application of Fe_3O_4@C

5.1 Oxidation of 5-HMF

Since Fe_3O_4 has been successfully used in many oxidation reactions with good selectivity towards the desired product [43, 44] it has been initially evaluated in the aerobic oxidation of 5-HMF. A little conversion of HMF took place in toluene or in aqueous medium in the absence of a base using air as an oxidant (Table 2, Entries 1–3). A combination of metal and base catalyzed oxidation reactions of 5-HMF have been reported, especially using potassium carbonate [45]. No conversion of 5-HMF took place using only magnetite at 100 °C without addition of a base. However in the presence of potassium carbonate, 5-HMF was converted into DFF with 94.8% selectivity (Table 2, Entry 4). In the presence of hydrogen peroxide 56% of HMF was converted with 55.4% selectivity to DFF in toluene whereas in water 86.4% of HMF was converted with 95.4% selectivity to DFF. By lowering the temperature to 80 °C, conversion of HMF decreased to 74.8% with

Table 2 Oxidation of 5-HMF to DFF catalysed by Fe_3O_4 and Fe_3O_4@C

Entry	Catalyst	Base	Solvent	Oxidant	Temp. (°C)	Time (h)	HMF conv. (%)	DFF selectivity (%)
1	Fe_3O_4	–	Toluene	Air	100	72	< 10	–
2	Fe_3O_4	K_2CO_3	Toluene	Air	100	72	< 10	–
3	Fe_3O_4	–	Water	Air	100	72	–	–
4	Fe_3O_4	K_2CO3	Water	Air	100	72	58.0	94.8
5	Fe_3O_4	K_2CO3	Toluene	H_2O_2	100	72	56.0	55.4
6	Fe_3O_4	K_2CO_3	Water	H_2O_2	100	72	86.4	95.4
7	Fe_3O_4	K_2CO_3	Water	H_2O_2	80	72	74.8	95.2
8	CNPs	K_2CO_3	Water	Air	100	72	–	–
9	Fe_3O_4@C	–	Toluene	Air	100	12	< 1	< 1
10	Fe_3O_4@C	–	Toluene	Air	100	12	< 1	< 1
11	Fe_3O_4@C	–	water	Air	100	12	< 1	< 1
12	Fe_3O_4@C	–	DMF	Air	100	12	< 1	< 1
13	Fe_3O_4@C	–	DMSO	Air	100	12	< 1	< 1
14	Fe_3O_4@C	–	water	H_2O_2	100	12	< 1	< 1
15	Fe_3O_4@C	K_2CO_3	Water	H_2O_2	80	72	93.0	78.7
16	Fe_3O_4@C	K_2CO_3	Water	Air	80	72	96.2	95.4
17	Fe_3O_4@C	K_2CO_3	Water	O_2	80	72	98.0	95.6
18	Fe_3O_4@C	K_2CO_3	Water	H_2O_2	RT	72	35.0	11
19	Fe_3O_4@C	–	Acetonitrile	TEMPO	100	24	6.0	< 1
20	Fe_3O_4@C	K_2CO_3	Acetonitrile	TEMPO	100	72	63.0	74.6
21	Fe_3O_4@C	–	Water	TEMPO	80	72	< 1	< 1
22	Fe_3O_4@C	K_2CO_3	Water	TEMPO	80	72	95.0	98.0

Reaction conditions: substrate (0.25 mmol), catalyst (5.0 mg), K_2CO_3 (27.5 mg), solvent (5.0 mL). Conversion and selectivity are calculated based on HPLC

almost same selectivity to DFF (Table 2, Entry 5 and 6). To understand the effect of CNPs, oxidation of 5-HMF was carried out using Fe_3O_4@C. The best conditions to obtain the maximum conversion of HMF is 96.2% with 95.4% selectivity to DFF in the presence of air (Table 2, Entries 15–18). Reactions in strongest polar solvents such as water produced much higher HMF conversion than other solvents. It may be due to the possible reason should be that water can well disperse Fe_3O_4@C and good solubility of HMF. Although the rate of the reaction increases by the presence of CNPs on magnetite, selectivity to DFF remains the same as with Fe_3O_4 and Fe_3O_4@C. (Table 2). The better performance of Fe_3O_4@C may be due to hydrophobic nature of CNPs accommodated inside the magnetite, which may leads to the formation of crystal defects and hence higher activity. In general oxidation of 5-HMF in low boiling aprotic solvent like acetonitrile proved as a best solvent using TEMPO as an oxidant [46]. Therefore the oxidation reaction was conducted in acetonitrile using TEMPO as an oxidant and best result was obtained with 98% selectivity at the cost of 95% conversion at 80 °C (Table 1, Entries 19–22). Notably, the reaction did not produce any product under catalyst free conditions. Besides DFF, a trace amount of the other oxidation product 5-hydroxymethyl-2-furancarboxylic acid (HMFCA), levulinic acid (LA) were also detected by HPLC, which indicates that DFF is stable in water in presence of the Fe_3O_4@C under the reaction conditions employed in this work. Control experiments were also performed to understand insights into the conversion of HMF.

5.2 Direct Conversion of Biomass

The potentiality of our hybrid catalyst, Fe_3O_4@C has been explored directly in the one pot synthesis of DFF directly either from glucose or fructose [47–49] (Scheme 2).

Using glucose as a substrate in the aqueous medium DFF was obtained with 99.3% selectivity using hydrogen peroxide and it is also highly remarkable that HMF which was formed (in situ) reacted completely. Moreover in the presence of air, there was no HMF remained in the flask after 72 h and DFF was obtained with 84.3% selectivity. Significantly, DFF has been obtained with 94.8% selectivity with complete conversion of fructose at 80 °C. Of particular note is that no catalytic conversion of either glucose or fructose has taken place using magnetite alone (Table 3, Entry 5 and 6). This result clearly indicates that Fe_3O_4@C acts as a bifunctional catalyst where the subsequently dehydration and oxidation reactions took place. Moreover CNPs on Fe_3O_4 demonstrates much superior catalytic activity than the un-doped iron oxide suggesting that the introduction of CNPs into Fe_3O_4 played a crucial role in dehydration step. The higher activity of this hybrid catalyst is also may be due to carbon particles (from the candle soot) on Fe_3O_4 resulted in a better Fe^{3+} adsorption and enhanced dispensability. The superior activity exhibited by Fe_3O_4@C is may also due to facile redox reaction of Fe^{3+} to Fe^{2+} occurs in an easier way because of the synergetic effects of CNP on inverse spinel Fe_3O_4 and thus reaction proceeds smooth way. To the best of our knowledge this is the first report to synthesize the highly active catalyst using candle soot for biomass conversion. The acidic hydroxyls of 5-HMF might have a strong interaction with Fe_3O_4, which may leads to lower activity in the biomass conversion.

Table 3 Conversion of biomass into DFF catalyzed by Fe_3O_4@C

S. no	Substrate	Catalyst	Oxidant	HMF (%)	DFF (%) selectivity
1	Glucose	Fe_3O_4@C	H_2O_2	–	99.3
2	Glucose	Fe_3O_4@C	Air	–	84.3
3	Fructose	Fe_3O_4@C	H_2O_2	< 1%	73.8
4	Fructose	Fe_3O_4@C	Air	< 2%	94.8
5	Glucose	Fe_3O_4	H_2O_2	–	–
6	Fructose	Fe_3O_4	H_2O_2	–	–

Reaction condition: Substrate (1.0 mmol), Catalyst (5.0 mg), K_2CO_3 (27.5 mg), H_2O (5.0 mL)

Scheme 2 Fe_3O_4@C catalyzed biomass to DFF

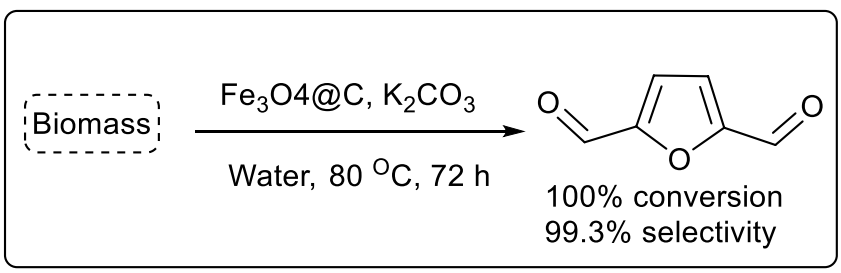

6 Conclusions

In summary, we developed a highly active new heterogeneous catalyst in a simple way by utilizing candle soot, which is known as a pollutant. In our protocol pollutant material was converted into useful material for the development of sustainable catalyst on the magnetite, *i.e.* Fe_3O_4@C. It is well characterized through various techniques using PXRD, XPS and Raman analysis. The SEM–EDS analysis further confirms the successful preparation of this hybrid material. Further this material is operable under mild conditions for the selective oxidation of HMF to DFF with high selectivity. In this process water, a greener solvent showed better performance which circumvents the use of high boiling solvents at higher temperatures. Further, the absence of precious noble metals and simple preparation of catalyst makes catalytic protocol attractive for the conversion of biomass into value added products via two consecutive steps such as dehydration and oxidation reactions. Fe_3O_4@C plays a major role in the dehydration reaction of biomass whereas Fe_3O_4 alone could not catalyzed. Our work will stimulate a lot of further research on the design of new heterogeneous catalysts and the elucidation of the underlying modes of action.

Supplementary Information The online version contains supplementary material available at https://doi.org/10.1007/s10904-021-02062-6.

Acknowledgements KVSR thanks to CSIR for providing the financial support acknowledged to CSIR project number [01(2968)/19/EMR-II]. Kind acknowledgements to Dr. Melad Shaikh for his suggestions. Kind acknowledgements to BHU for providing facilities of PXRD, FT-IR, Raman and XPS analysis and IIT-Kharagpur for SEM-EDX.

References

1. Z. Zhang, J. Song, B. Haun, Chem. Rev. **117**, 6834–6880 (2017)
2. C. Moreau, M.N. Belgacem, A. Gandini, Top. Catal. **27**, 11–30 (2004)
3. X. Kong, Y. Zhu, Z. Fang, J. Kozinski, I.S. Butler, L. Xu, H. Song, X. Wei, Green Chem. **20**, 3657–3682 (2018)
4. T. Xiang, X. Liu, P. Yi, M. Guo, Y. Chen, C. Wesdemiotis, J. Xu, Y. Pang, Polym. Int. **62**, 1517–1523 (2013)
5. K.T. Hopkins, W.D. Wilson, B.C. Bendan, D.R. McCurdy, J.E. Hall, R.R. Tidwell, A. Kumar, M. Bajic, D.W. Boykin, J. Med. Chem. **41**, 3872–3878 (1998)
6. A.S. Amarasekara, D.G. LaToya, D. Williams, Eur. Polym. J. **45**, 595–598 (2009)
7. K. Weissermel, H.J. Arpe, *Industrial Organic Chemistry* (VC-Wiley, Weinheim, 1997), p. 225
8. Q.-S. Kong, X.-L. Li, H.-J. Xu, Y. Fu, Fuel Process. Technol. **209**, 106528 (2020)
9. X. Li, L. Zhang, S. Wang, Y. Wu, Front. Chem. **7**, 748 (2019)
10. J. Ma, Z. Du, J. Xie, Q. Chu, Y. Pang, Chemsuschem **4**, 51–54 (2011)
11. J. Nie, J. Xie, H. Liu, J. Catal. **301**, 83–91 (2013)
12. Z. Zhang, Z. Yuan, D. Tang, Y. Ren, K. Lv, B. Liu, Chemsuschem **7**, 3496–3504 (2014)
13. X. Tong, L. Yu, H. Chen, X. Zhuang, S. Liao, H. Cui, Catal. Commun. **90**, 91–94 (2017)
14. Z. Yaun, B. Liu, P. Zhou, Z. Zhang, Q. Chi, Catal. Sci. Technol. **8**, 4430–4439 (2018)
15. J. Nie, H. Liu, J. Catal. **316**, 57–66 (2014)
16. F. Neatu, N. Petrea, R. Petre, V. Somoghi, M. Florea, V.I. Parvulescu, Catal. Today **278**, 66–73 (2016)
17. Z. Gui, S. Sarvanumurughan, W. Cao, L. Schill, L. Chen, Z. Qi, A. Riisager, ChemistrySelect **2**, 6632–6639 (2017)
18. S. Biswas, B. Dutta, A.M. Kannakithodi, R. Clarke, W. Song, R. Ramprasad, S.L. Suib, Chem. Commun. **53**, 11751–11754 (2017)
19. J. Chen, Y. Guo, J. Chen, L. Song, L. Chen, ChemCatChem. **6**, 3174–3181 (2014)
20. C. Carlini, P. Patrono, A.M.R. Galletti, G. Sbrana, V. Zima, Appl. Catal. A: Gen. **289**, 197–204 (2005)
21. O.C. Navarro, A.C. Canos, S. Chornet, Top. Catal. **52**, 304–314 (2009)
22. I. Sadaba, Y.Y. Gorbanev, S. Kegnaes, S.S.R. Putluru, R.W. Berg, A. Riisager, ChemCatChem **5**, 284–293 (2013)
23. N.-T. Le, P. Lakshmanan, K. Cho, Y. Han, H. Kim, Appl. Catal. A: Gen. **464–465**, 305–312 (2013)
24. Z. Yang, W. Qi, R. Su, Z. He, Energy Fuels **31**, 533–541 (2017)
25. B. Liu, Z. Zhang, K. Lv, K. Deng, H. Duan, Appl. Catal. A: Gen. **472**, 64–71 (2014)
26. Z. Yang, W. Qi, R. Su, Z. He, ACS Energy Fuels **31**, 533–541 (2017)
27. R. Fang, R. Luque, Y. Li, Green Chem. **18**, 3152–3157 (2016)
28. C. Cha, S.R. Shin, N. Annabi, M.R. Dokmeci, A. Khademhosseini, ACS Nano **7**, 2891–2897 (2013)
29. D. Jariwala, V.K. Sangwan, L.J. Lauhon, T.J. Marks, M.C. Hersam, Chem. Soc. Rev. **42**, 2824–2860 (2013)
30. F.M. Abel, S. Pourmiri, G. Basina, V. Tzitzios, E. Devlin, G.C. Hadjipanayis, Nanoscale Adv. **1**, 4476–4480 (2019)
31. F. Li, S. Jiang, J. Haung, Y. Wang, S. Lu, C. Li, New J. Chem. **44**, 478–486 (2020)
32. J. Zheng, Z.Q. Liu, X.S. Zhao, M. Liu, X. Liu, W. Chu, Nanotechnology **23**, (2012)
33. A. Jafari, K. Boustani, S. Farjami Shayesteh, J. Supercond. Nov. Magn. **27**, 187–194 (2014)
34. L. Wang, Y. Yu, P.C. Chen, D.W. Zhang, C.H. Chen, J. Power Sources **183**, 717–723 (2008)
35. N. Zhao, S. Wu, C. He, Z. Wang, C. Shi, E. Liu, J. Li, Carbon **57**, 130–138 (2013)
36. C. Yang, Z. Li, Y. Haung, K. Wang, Y. Long, Z. Guo, X. Li, H. Wu, Nano Lett. **21**, 3198–3204 (2021)
37. Z. Su, W. Zhou, Y. Zhang, Chem. Commun. **47**, 4700–4702 (2011)
38. H. Liu, T. Ye, C. Mao, Angew. Chem. Int. Ed. **46**, 6473–6475 (2007)
39. M.R. Mulay, A. Chauhan, S. Patel, V. Balakrishnan, A. Halder, R. Vaish, Carbon **144**, 684–712 (2019)
40. M. Ventura, A. Dibenedetto, M. Aresta, See the review on heterogeneous catalysis in water for DFF. Inorg. Chim. Acta **470**, 11–21 (2018)
41. H. Du, F. Deng, R.R. Kommalapati, A.S. Amarasekhara, Renew. Sustain. Energy Rev. **134**, 110292 (2020)
42. P.C. Panta, C.P. Bergmann, J. Mater. Sci. Eng **5**, 217 (2015)
43. M. Shaikh, M. Satanami, K.V.S. Ranganath, Catal. Commun. **54**, 91–93 (2014)
44. M. Shaikh, M. Sahu, P.K. Gavel, K.V.S. Ranganath, Catal. Commun. **64**, 18–21 (2015)
45. P. Pal, S. Saravanamurugan, Chemsuschem **12**, 145–163 (2019)

46. N. Mittal, G.M. Nisola, L.B. Malihan, J.G. Seo, S.-P. Lee, W.-J. Chung, Korean J. Chem. Eng. **31**, 1362–1367 (2014)
47. C. Laugel, B. Estrine, J.L. Bras, N. Hoffmann, S. Marinkovic, J. Muzart, ChemCatChem **6**, 1195–1198 (2014)
48. Z.-Z. Yang, J. Deng, T. Pan, Q.-X. Guo, Y. Fu, Green Chem. **14**, 2986–2989 (2012)
49. X. Xiang, L. He, Y. Yang, B. Guo, D. Tong, C. Hu, Catal. Lett. **141**, 735–741 (2011)